# β-decay properties of the very neutron-rich isotopes ^{86}Ge and ^{86}As

C. Mazzocchi, K. P. Rykaczewski, R. Grzywacz, P. Bączyk, C. R. Bingham, N. T. Brewer, C. J. Gross, C. Jost, M. Karny, A. Korgul, M. Madurga, A. J. Mendez, II, K. Miernik, D. Miller, S. Padgett, S. V. Paulauskas, A. A. Sonzogni, D. W. Stracener, and M. Wolińska-Cichocka

Phys. Rev. C **92**, 054317 — Published 19 November 2015

DOI: 10.1103/PhysRevC.92.054317

# $\beta$-decay properties of the very neutron-rich isotopes $^{86}$Ge and $^{86}$As*

C. Mazzocchi,[1] K.P. Rykaczewski,[2] R. Grzywacz,[3,2] P. Bączyk,[1] C.R. Bingham,[3,2] N.T. Brewer,[4,2,5] C.J. Gross,[2] C. Jost,[3] M. Karny,[1,6] A. Korgul,[1] M. Madurga,[3] A.J. Mendez II,[2] K. Miernik,[2,1] D. Miller,[3] S. Padgett,[3] S.V. Paulauskas,[3] A.A. Sonzogni,[7] D.W. Stracener,[2] and M. Wolińska-Cichocka[2,6,8]

[1] *Faculty of Physics, University of Warsaw, PL 02-093 Warsaw, Poland*
[2] *Physics Division, Oak Ridge National Laboratory, Oak Ridge, TN 37831, USA*
[3] *Department of Physics and Astronomy, University of Tennessee, Knoxville, TN 37996, USA*
[4] *Department of Physics and Astronomy, Vanderbilt University, Nashville, TN 37235, USA*
[5] *Joint Institute for Nuclear Physics and Applications, Oak Ridge, TN 37831, USA*
[6] *Oak Ridge Associated Universities, Oak Ridge, TN 37831, USA*
[7] *National Nuclear Data Center, Brookhaven National Laboratory, Upton, NY 11973, USA*
[8] *Heavy Ion Laboratory, University of Warsaw, Warsaw, PL 02-093, Poland*

The $\beta$ decay properties of very neutron rich nuclei $^{86}$Ge and $^{86}$As were measured at the Holifield Radioactive Ion Beam Facility at Oak Ridge National Laboratory. Spectroscopic information on new excited states in $^{86}$As and in $^{86}$Se was obtained and is interpreted within an advanced shell model approach. These calculations, previously explaining well the structure of $^{84}$Ge and $^{85}$Ge, are not able to reproduce all the experimentally-determined features of the measured level schemes of $^{86}$As and $^{86}$Se. The Gamow-Teller decay of $^{86}$Ge and $^{86}$As is also investigated in a shell-model framework. The fission yield for $^{86}$Ge is discussed.

PACS numbers: 23.40.-s, 23.20.lv, 27.50.+e, 25.85.Ge

## I. INTRODUCTION

Measurement of the properties of nuclei with large N/Z ratios and theoretical description of their structure is one of the most important topics in modern nuclear physics. Excess of neutrons can give rise to evolution in the single particle energies and consequently lead to changes in the shell structure. The nuclear levels can be reorganized in a different energy sequence than they are in isotopes closer to the $\beta$-stability line. Such evolution is reflected also in the decay properties of these exotic nuclei. In the most recent years progress in experimental techniques has allowed access to very exotic isotopes and made possible detailed studies on nuclei never before investigated. In particular, the region of the chart of nuclei beyond the double shell closure at N=50 and Z=28 provided a very fertile playground for such investigations. The study of $\beta$-decay of these nuclei gives the unique possibility to probe our understanding of these very exotic isotopes by investigating the evolution of the structure of excited levels and decay properties, and testing theoretical predictions, in particular those given by the nuclear shell model.

In this context we have investigated the decay properties of the two very exotic A=86 isobars, $^{86}$Ge and its daughter $^{86}$As. Figure 1 depicts the decay path followed by $^{86}$Ge relevant to this work, i.e. ending with the selenium isotopes. Before this measurement, a few events of $^{86}$Ge had been observed in projectile fission of $^{238}$U and a lower limit of 150 ns for its half-life was established [1]. Part of the data, namely the half-life measurement, was published in Ref. [2] and preliminary data on excited states in $^{86}$Se in Ref. [3].

## II. EXPERIMENTAL TECHNIQUE

A high-purity beam of radioactive $^{86}$Ge was produced at the Holifield Radioactive Ion Beam Facility at Oak Ridge National Laboratory (HRIBF) [5]. The experimental technique was described in detail in Ref. [2]. In brief, the $^{86}$Ge ions were produced in the proton-induced fission of $^{238}$U and ionized to a charge state +1 in the Injector for Radioactive Ion Species 2 (IRIS2) ion source. Two-stage electromagnetic separation and ion-source chemistry suppressed many of the A=86 contaminants and resulted in a beam where $^{86}$Ge constituted ~18% of the beam cocktail, with $^{86}$As forming the remaining ~82%. The beam was directed to the measuring station, where the detection set-up was positioned. The latter consisted of the moving tape collector (MTC), into which the ions were implanted. Its role was to periodically remove the accumulated sample from the collection region, thus suppressing the longer-lived daughter activity which could otherwise be observed by the detection system. Moreover, the beam was periodically deflected away by an electrostatic deflector. A cycle of 1.5 s *beam-on*, 1.0 s *beam-off* and 0.36 s tape-transport time was applied for this measurement. The implantation point was surrounded by two plastic scintillators and four HPGe clover detectors in close ge-

* Notice: This manuscript has been authored by UT-Battelle, LLC, under Contract No. DE-AC05-00OR22725 with the U.S. Department of Energy. The United States Government retains and the publisher, by accepting the article for publication, acknowledges that the United States Government retains a non-exclusive, paid-up irrevocable, world-wide license to publish or reproduce the published form of the manuscript, or allow others to do so, for United States Government purposes.

ometry. The photo peak efficiency for the clover array was 6% at 1.3 MeV and 32% at 100 keV. The $\beta-$detection efficiency was determined for each of the transitions of interest by comparing the number of counts in the $\beta\gamma$ and $\gamma-$singles sum spectra for the given peak. When the lines in the $\gamma-$singles spectra were too weak or not visible, $\gamma\gamma$ coincident spectra were used: intensities of the $\gamma-$gated peaks from $\beta\gamma\gamma$ and $\gamma\gamma$ matrices were compared. The values of the $\beta$-detection efficiency were calculated for each $\gamma$-transition and all of them turned out to be compatible with $\epsilon_\beta$=50%, within error bars. All signals were read out by a digital-electronics-based data acquisition system [6, 7] utilizing XIA Pixie16 Rev. D modules [8].

## III. RESULTS

The $\beta$-gated $\gamma$-ray spectrum acquired at mass 86 is displayed in Figure 2. Several new transitions were identified and assigned to the $\beta\gamma$ and $\beta$-delayed neutron-$\gamma$ ($\beta n\gamma$) decay branches of $^{86}$Ge ($T_{1/2}$=226(21) ms) and $^{86}$As ($T_{1/2}$=861(64) ms) [2].

### A. $^{86}$Ge $\beta$-decay

The most intense line in $^{86}$Ge $\beta$ decay, at 112 keV, was assigned to its $\beta\gamma$ decay-branch on the basis of half-life

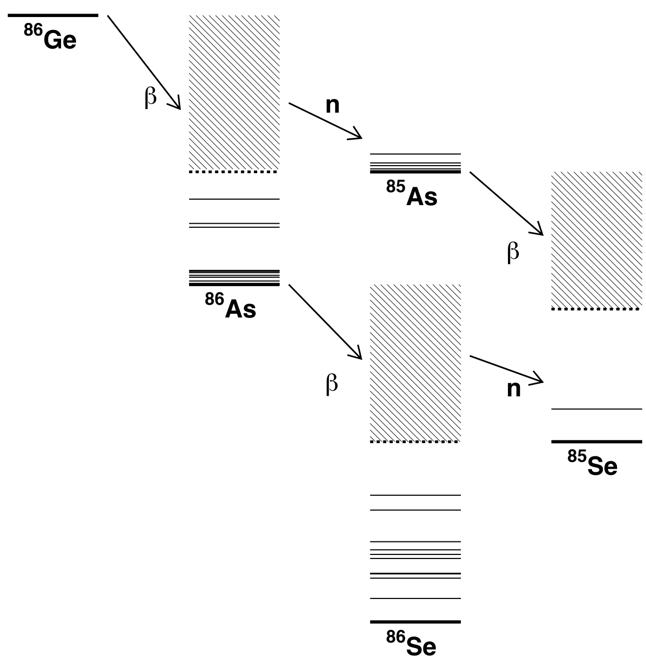


FIG. 1. Schematic decay path of $^{86}$Ge. Energies are to scale and the presented discrete levels (solid lines) are from this work. $Q_\beta$ values and neutron-separation energies ($S_n$, dashed lines) are taken from [4]. Neutron-unbound states are represented by the shaded regions.

considerations, ion-source chemistry and mass separation [2]. All the other transitions including those at 98, 119, 125 and 1965 keV visible in the $\beta\gamma$ spectrum (see Figure 2), as well as those detected only with the help of an additional $\gamma$ coincidence (see, e.g., Figures 3 and 4), were assigned to the same decay by means of $\beta\gamma\gamma$ coincidences. Two transitions at 178 and 441 keV were also assigned to the decay of $^{86}$Ge on the basis of their respective half-lives, 290(70) and 190(150) ms. They most likely de-excite levels in the $\beta\gamma$ daughter $^{86}$As, but could not be placed in the level scheme.

Four transitions at 102, 116, 206 and 396 keV were identified as following the $\beta$n decay of $^{86}$Ge to $^{85}$As, the most intense of which are visible also in the $\beta\gamma$ spectrum (see Figure 2). Their assignment to the $\beta n\gamma$ decay-branch is based on the known properties of excited states in $^{85}$As [9, 10] and on $\beta\gamma\gamma$ coincidences.

The partial $\beta$-decay scheme of $^{86}$Ge (see Figure 5) could be reconstructed on the basis of the $\gamma$-transition assignments, coincidence schemes and relative intensities described above and summarized in detail in Table I. A proposal for tentative spin and parity for the lowest-lying levels in $^{86}$As, see Figure 5, results from the following considerations.

For $^{86}_{33}$As$_{53}$, low-energy transitions (E≤150 keV) with multipolarity $E2$ or larger are expected to have lifetimes longer than several hundreds of nanoseconds [13]. If we take into account the correction factors to the lifetimes from systematics [14, 15], the lifetime would still be long enough to be isomeric. Since no isomeric behavior with lifetimes longer than a hundred nanoseconds was observed in the data for the low energy transitions, dipole character could be inferred.

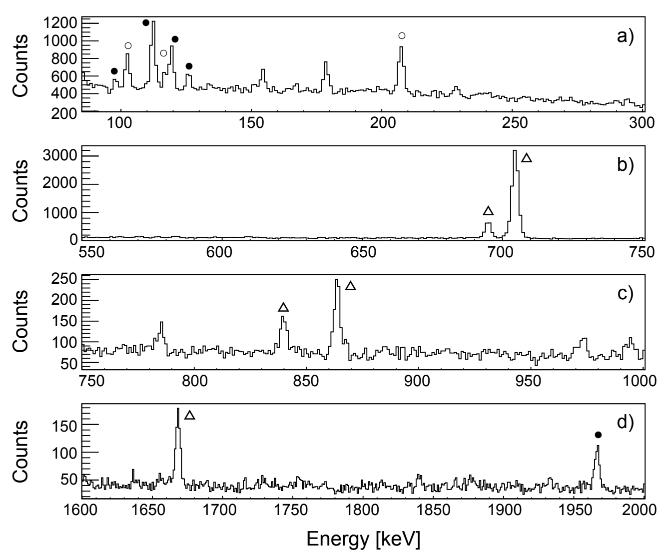


FIG. 2. Parts of the $\beta$-gated $\gamma$-ray spectrum of mass 86 (background subtracted). $\gamma$ lines belonging to the $\beta\gamma$ (●) and $\beta n\gamma$ (◯) decay branches of $^{86}$Ge are marked, as well as those belonging to the $\beta\gamma$ decay of $^{86}$As (△). Unmarked lines belong to room- and beam-induced background. See text for details.

In the spherical limit, the five protons and three neutrons outside the double shell closure at Z=28 and N=50 will occupy orbitals with negative ($\pi p_{3/2}$ or $\pi f_{5/2}$) and positive ($\nu g_{7/2}$ or $\nu d_{5/2}$) parity, generating low-lying negative-parity states. Indeed, no positive-parity levels are expected at energies lower than ~2.5 MeV [16]. Therefore the low-energy transitions at the bottom of $^{86}$As level scheme will have predominantly M1 character.

The potential $\beta$-feeding of the $^{86}$As ground state (g.s.) and of the two low-energy states at 7 keV and 21 keV was considered in the $\beta$ feeding budget, see Figure 5. The apparent $\beta$-feeding ($I_\beta$) values were calculated taking the following into account.

- The $\beta$n decay-branch was measured to be $P_n$=45(15)% [11], which results in 55(15)% for $\beta$ transitions to the states in $^{86}$As.
- A first-forbidden ($ff$) character of $\beta$ transitions to the g.s. and two lowest excited states was adapted, since no positive parity states are expected at such low excitation energies and the even-even $^{86}$Ge has $I^\pi=0^+$ g.s. If, in line with the $log(ft)$ values known in this region for $ff$ transitions, we assume a typical $log(ft)$ of 7.0−6.0 for the decay to any of these states, a feeding of 0.4−4% can be inferred to each of them.
- The relative $\gamma$ intensities (see Table I) were normalized to the sum of all intensities feeding the three lowest-lying states in $^{86}$As. The relatively intense 178 keV and 441 keV transitions, for which no $\gamma\gamma$ coincidences with any of the assigned lines were detected, were assumed to populate the low energy level "triplet" (g.s., 7 keV, 21 keV). Therefore, their intensities were added to the intensities of 119 keV, 112 keV and 98 keV transition when

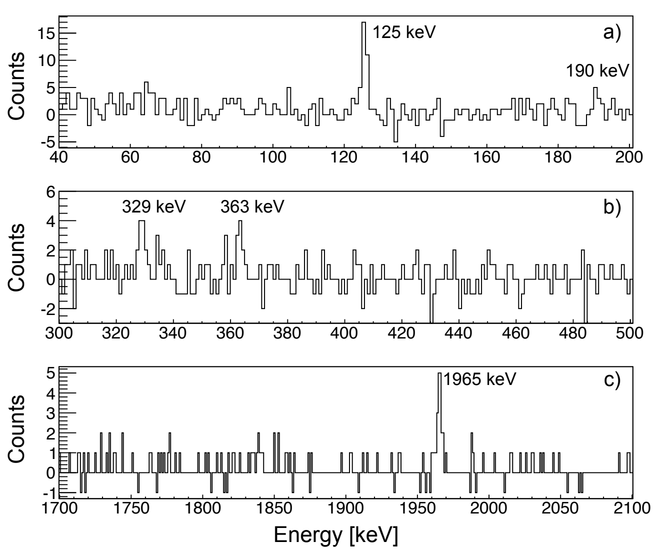


FIG. 3. Parts of the $\beta$-gated $\gamma$-ray spectrum (background subtracted) in coincidence with the 112 keV transition. See text for details.

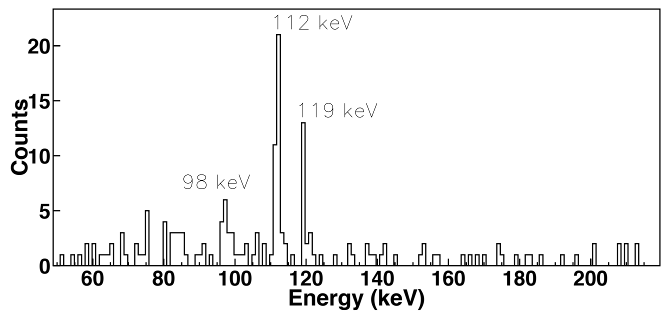


FIG. 4. Low-energy part of the $\beta$-gated $\gamma$-ray spectrum (background subtracted) in coincidence with the 125 keV transition. See text for details.

TABLE I. Properties of the $\gamma$-ray transitions following the $\beta$ decay of $^{86}$Ge. The $\gamma$-ray intensities ($I_\gamma^{TOT}$) are normalized to the 112 keV transition.

| Energy keV | Decay branch | $I_\gamma^{TOT}$ % | Coincidences keV |
|---|---|---|---|
| 97.6(5) | $\beta\gamma$ | 12(3)$^d$ | 125.4, 1965.4 |
| 111.8(3) | $\beta\gamma$ | 100(7)$^d$ | 125.4, 190.3, 283.6, 328.5, 362.9, 1965.4, 2798 |
| 118.9(3) | $\beta\gamma$ | 60(8)$^d$ | 125.4, 1965.4 |
| 125.4(3) | $\beta\gamma$ | 24(4)$^d$ | 97.6, 111.8, 118.9 |
| 190.3(3)$^a$ | $\beta\gamma$ | 8(2)$^d$ | 111.8 |
| 283.6(5)$^a$ | $\beta\gamma$ | 6(2) | 111.8 |
| 328.5(5)$^a$ | $\beta\gamma$ | 14(4) | 111.8 |
| 362.9(5)$^a$ | $\beta\gamma$ | 12(3) | 111.8 |
| 1965.4(3)$^b$ | $\beta\gamma$ | 67(11)$^f$ | 97.6, 111.8, 118.9 |
| 2798(1)$^a$ | $\beta\gamma$ | 21(10) | 111.8 |
| | | | |
| 102.0(3) | $\beta$n | 50(6)$^e$ | 116.4, 206.3, 395.5 |
| 116.4(3) | $\beta$n | 23(4)$^e$ | 102.0, 395.5 |
| 206.3(3)$^b$ | $\beta$n | 14(3)$^{e,f}$ | 102.0 |
| 395.5(5)$^a$ | $\beta$n | 8(2)$^f$ | 102.0, 116.4 |
| | | | |
| 178.1(3)$^c$ | $\beta\gamma$ or $\beta n$ | 53(8)$^e$ | 240.5, 295.2 |
| 240.5(5)$^{a,c}$ | $\beta\gamma$ or $\beta n$ | — | 178.1 |
| 295.2(5)$^{a,b,c}$ | $\beta\gamma$ or $\beta n$ | — | 178.1 |
| 441.1(3)$^c$ | $\beta\gamma$ or $\beta n$ | 30(5) | — |

$^a$ Transition observed only in coincidence.
$^b$ Doublet resolved with $\beta\gamma\gamma$ coincidences.
$^c$ Transition not placed in the level scheme.
$^d$ The intensity is corrected for internal conversion (IC) assuming M1 character (see text for details): $\alpha_{TOT}$(98 keV)=0.0961(14), $\alpha_{TOT}$(112 keV)=0.0665(10), $\alpha_{TOT}$(119 keV)=0.0563(8), $\alpha_{TOT}$(125 keV)=0.0488(7), $\alpha_{TOT}$(190 keV)=0.0164(2) [12].
$^e$ Apparent intensity, value not corrected for IC.
$^f$ Intensity obtained from coincidences.

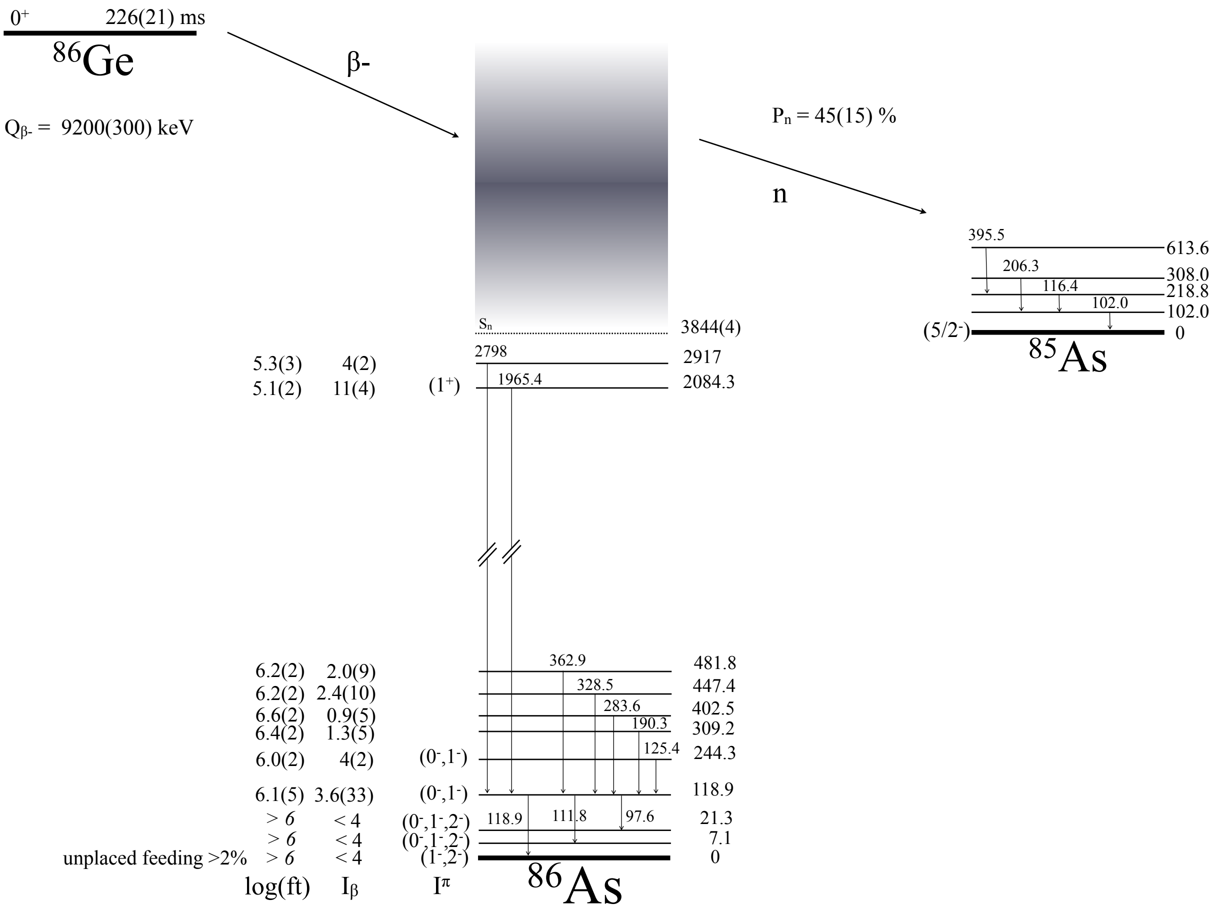


FIG. 5. Schematic representation of $^{86}$Ge $\beta$ decay. Energies are given in keV, apparent $\beta$-feedings (I$_\beta$) in %. Q-values and neutron-separation energy (S$_n$) stem from [4], half-life from [2] and P$_n$ from [11]. Neutron-unbound states are represented by the shaded regions. Drawing not to scale. See text for details.

making the $\beta$ intensity budget. For the direct I$_\beta$ of the triplet states we take an upper limit of 12%, leaving 43(15)% for the sum of 98 keV, 112 keV, 119 keV, 178 keV and 441 keV transitions.

Only those excited states with I$_\beta$$\sim$3% or larger were considered for tentative spin/parity assignment. Apparent $log(ft)$ values were calculated (see Figure 5) and the systematics of $log(ft)$ values for $0^+\!\rightarrow\!0^-$, $0^+\!\rightarrow\!1^-$ and $0^+\!\rightarrow\!2^-$ $\beta$-transitions were considered for guidance [17].

The low-energy negative-parity states at 119 and 244 keV can be fed by means of first-forbidden ($ff$) transitions, hence I$^\pi$=($0^-$, $1^-$). The 2084 keV level might be populated by an allowed Gamow-Teller (GT) transition, hence I$^\pi$=($1^+$), given the much larger I$_\beta$ with respect to the other observed levels and considering that positive parity states cannot be excluded at these higher excitation energies. Any transition between the 21.3 keV, 7.1 keV and the g.s. levels is going to be converted and the feeding to the individual levels cannot be disentangled directly from the data. Considering that I$_\beta$ to each of the three levels is $\leq$ 4%, $ff$-unique transitions cannot be excluded: I$^\pi$(21.3, 7.1 keV)=($0^-$, $1^-$,$2^-$). The apparent g.s. of $^{86}$As seems to decay with sizable I$_\beta$ to the I$^\pi$=$2^+$ first excited state and to the I$^\pi$=($2_2^+$) at 1398.6 keV in $^{86}$Se (see Section III B and Figure 6). This points towards I$^\pi$=($1^-$,$2^-$) for the g.s. of $^{86}$As.

As far as the $\beta$n decay branch is concerned, feeding to several excited states in $^{85}$As was observed. Unfortunately no spin/parity could be inferred to them, thus hindering the possibility to determine $\beta n\gamma$ intensities and delayed neutron branching to individual excited states (multi-polarities for the low-energy $\gamma$-transitions are not known).

### B. $^{86}$As $\beta$-decay

As-86 nuclei were present at the beam-implantation spot both as decay-daughter of $^{86}$Ge and as a mass contaminant. Most arsenic was indeed highly suppressed by the combination of ion-source chemistry with the use of molecular beams and high-resolution mass-separation, yet about 82% of $^{86}$As stemmed from isobaric contamination. This enabled the investigation of the $\beta$ decay

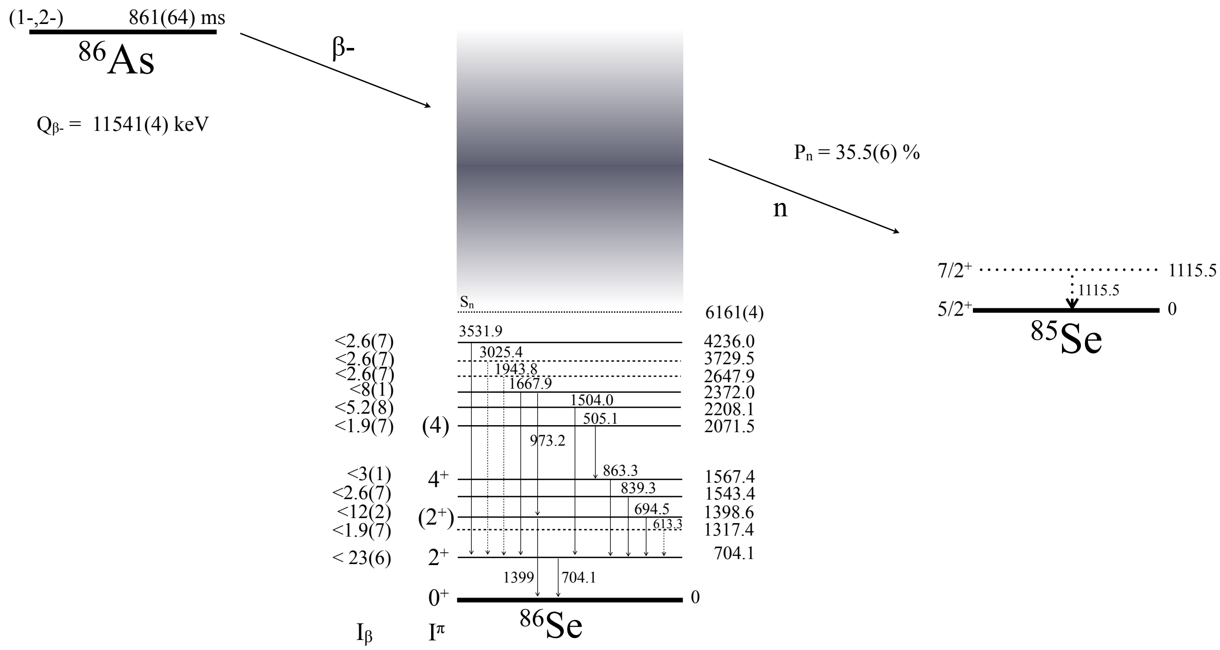


FIG. 6. Schematic representation of $^{86}$As $\beta$ decay. The level at 1115 keV in $^{85}$Se and the transition de-exciting it to the g.s. are depicted as dotted line and arrow, respectively. This is due to the fact that from this data it is not possible to disentangle the contributions to the 1115 keV transition from $\beta$n decay of $^{86}$As and from $\beta$ decay of $^{85}$As (see Figure 1). Energies are given in keV, I$_\beta$ in %; Q-values and S$_n$ stem from [4], half-life from [2] and P$_n$ from [18]. Upper limits for I$_\beta$ were determined by assuming no decay to the g.s. of $^{86}$Se and normalizing the relative $\gamma$ intensities to the 704 keV transition. Neutron-unbound states are represented by the shaded regions. Drawing not to scale. See text for details.

of $^{86}$As, leading to considerable improvement of the $^{86}$Se level scheme. Ten transitions were firmly assigned to the de-excitation of excited states in $^{86}$Se, only three of which were previously known either from $\beta$-decay studies of $^{86}$As (704 keV [19]) or prompt-$\gamma$ measurements in spontaneous fission of $^{252}$Cf (704, 863 and 505 keV [20, 21]). Correspondingly 8 new energy levels were established, see Figure 6. The assignment of the transitions is based on the coincidence scheme (see Table II and Figure 7). Two more transitions at 973 and 1399 keV were identified and assigned to de-excitations in $^{86}$Se on the basis of weak coincidences, level-energy differences and of the half-life value of 0.62(24)s for the 973 keV transition (see Table II). Moreover, the 1399 keV line was observed in the $\beta n\gamma$ decay of $^{87}$As [10].

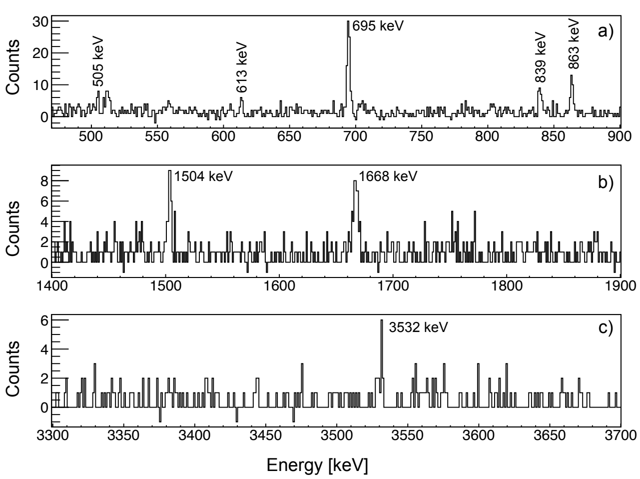


FIG. 7. Portions of the $\beta$-gated $\gamma$-ray spectrum (background subtracted) in coincidence with the 704 keV transition. See text for details.

The spin and parity of the 704.1, 1567.4 and 2071.5 excited states was determined before by Kratz et al. [19], Jones et al. [20] and Czerwiński et al. [21], respectively. Tentative I$^\pi$=(2$^+$) could be inferred for the 1398.6 keV level by taking into account:

- the apparent $\beta$ feeding, substantially larger than for other levels;
- the observation of a cross-over transition de-exciting from the 1398.6 level directly to the I$^\pi$=0$^+$ g.s.;
- the observation of this transition in the $\beta n\gamma$ decay of $^{87}$As [10];
- the fact that the level was not observed in the prompt-$\gamma$ fission data [21], where high-spin states yrast are expected to be populated.

TABLE II. Properties of the $\gamma$-ray transitions following the $\beta$ decay of $^{86}$As. The $\gamma$-ray intensities ($I_\gamma$) are normalized to the 704 keV transition.

| Energy keV | Decay branch | $I_\gamma$ % | Coincidences keV |
|---|---|---|---|
| 505.1(5) | $\beta\gamma$ | 3(1) | 704.1, 863.3 |
| 613.3(5)[a] | $\beta\gamma$ | 3(1) | 704.1 |
| 694.5(3) | $\beta\gamma$ | 18(2) | 704.1 |
| 704.1(3) | $\beta\gamma$ | 100(9) | 504.1, 613.3, 694.5, 839.3, 863.3, 1504.0, 1667.7, 1944, 3025, 3532 |
| 839.3(3) | $\beta\gamma$ | 4(1) | 704.1 |
| 863.3(3) | $\beta\gamma$ | 8(1) | 505.1, 704.1 |
| 973.2(5) | $\beta\gamma$ | 3(1) | 694.5, 704.1, 1399 |
| 1399(1)[b] | $\beta\gamma$ | – | 973.3 |
| 1504.0(3) | $\beta\gamma$ | 8(1) | 704.1 |
| 1667.9(5) | $\beta\gamma$ | 12(1) | 704.1 |
| 1944(1)[a] | $\beta\gamma$ | 4(1) | 704.1 |
| 3025(1)[a] | $\beta\gamma$ | 4(1) | 704.1 |
| 3532(1) | $\beta\gamma$ | 4(1) | 704.1 |
| 1115.5(3) | $\beta$n | 3.1(5) | – |

[a] Transition observed only in coincidence.
[b] Doublet resolved by means of $\beta\gamma\gamma$ coincidences.

### C. $^{86}$Ge fission yield

On the basis of the apparent decay scheme of $^{86}$Ge described above, we deduced a beam intensity for $^{86}$Ge at the measuring station of the order of 1 ion/s. This value, corrected for ion source efficiency (0.0002) for $^{86}$Ge ($T_{1/2}$=226(21) ms), for the sulfide formation probability (0.3), for the charge-exchange efficiency (0.3) and the transmission to the measuring station (0.5), gave a production yield of the order of $9\times10^3$ pps/$\mu$A for 50 MeV proton beam, which is more than 4 orders of magnitude lower than the production rate for the $^{86}$Br isobar ($4\times10^8$ pps/$\mu$A for 50 MeV proton beam [22]).

Ground-state $\beta$-decay properties of $^{86}$Ge such as its half-life and $\beta$n branching ratio, together with production yields of this isotope in thermal-neutron induced $^{235}$U fission listed in the ENDF, JENDL and JEFF data bases [23–25], were used recently for the sensitivity analysis for the kinetic behavior of a nuclear fission reactor [26]. The $^{86}$Ge g.s. properties input data for the calculations were taken from the JENDL compilation [24], i.e. $T_{1/2}$=88 ms and $P_n$=6%, while JEFF and ENDF assume $T_{1/2}$=300 ms and $P_n$=0 [25], and $T_{1/2}$=95 ms and $P_n$=5% [23], respectively. The conclusion of that work was that both yields and $\beta$-delayed properties of $^{86}$Ge should be verified and improved in order to obtain more reliable analysis. Recently we measured the half-life of $^{86}$Ge to be 226(21) ms [2] and estimated the delayed-neutron branching ratio as 45(15)% [11]. While the measured decay properties of $^{86}$Ge clearly differ from data bases values used in the sensitivity analysis [26], differences that are even larger arise if fission yields for $^{86}$Ge are taken from different data bases.

The independent fission yield for $^{86}$Ge in $n_{thermal}$+$^{235}$U is quoted as about $6.3\times10^{-3}$ in JENDL and ENDF, while it is three orders of magnitude lower in JEFF, $3\times10^{-6}$. Such discrepancy is not present in the isobar $^{86}$Br, which has yields at the level of $5\times10^{-3}$ to $7\times10^{-3}$ in all three data bases. It means that ENDF/JENDL list similar fission yields for $^{86}$Br (N=51) and for the much more neutron-rich nucleus $^{86}$Ge (N=54). Interestingly, the anomalously large yield for $^{86}$Ge triggered doubts as early as 1997 [27], but this value and similarly doubtful scattered yield values [28] still need to be verified.

In our studies of proton-induced fission of $^{238}$U we observe a yield for the production of $^{86}$Br that is almost five orders of magnitude larger than for $^{86}$Ge. This is close to the yield-ratio estimate given in JEFF, but very different from that obtained from the respective ENDF and JENDL values. The different fission mechanism (proton versus thermal neutron induced fission) and fissioning isotope ($^{238}$U versus $^{235}$U) is very unlikely to account for more than 4 orders of magnitude difference in the production yields.

## IV. DISCUSSION

### A. Low-energy excited states

In order to interpret the structure of the low-energy levels, we performed shell-model calculations for $^{86}$As and $^{86}$Se with the NuShellX code [16] using a model space containing all the active orbitals outside the $^{78}$Ni core and the N3LO residual interaction based on [29, 30] nucleon-nucleon forces. Similar calculations gave reliable predictions for excited states in very neutron-rich gallium isotopes [31].

In Figure 8 the prediction for the excitation energy of the lowest-lying excited states in $^{86}$As is plotted. Several low-spin states are expected at low-excitation energies in agreement with the experimental evidence. Nevertheless, the calculations do not manage to reproduce the level separation and grouping of states near the ground state as observed in the experiment, see Figure 5, nor the $^{86}$As g.s. spin, which is predicted to be $0^-$ and was determined to be ($1^-$,$2^-$), see Section III A. Candidates for $I^\pi$=$0^-$ are present close to the g.s. and such discrepancies are within the accuracy of the shell model predictions. It should not be forgotten that, since the radioactive $^{86}$Ge beam was not 100% pure ($^{86}$As contamination was present in the beam), the presence of $\beta$-decaying isomeric activities like $^{86m}$As in the A=86 beam cannot be excluded.

In Figure 9 the calculations performed for $^{86}$Se are shown. These predictions show better agreement with the experimental data displayed in Figure 6. The ex-

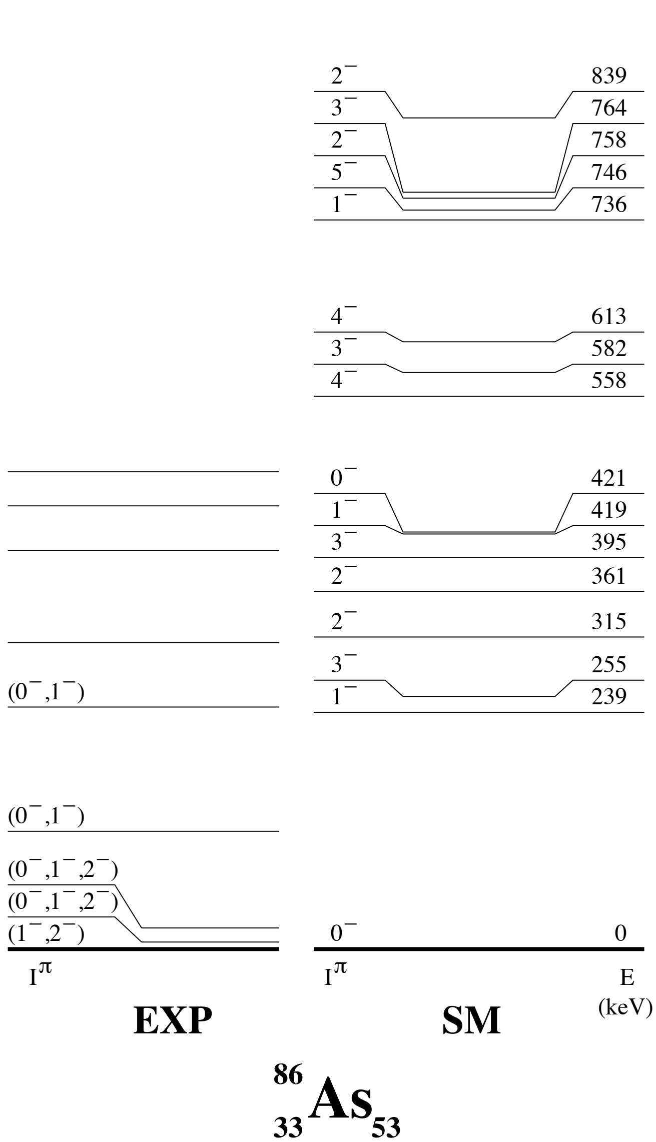


FIG. 8. Lowest-lying excited states in $^{86}$As predicted in shell-model calculations (SM) in comparison with the results of this work (EXP). The vertical (energy) axis is plotted to scale. See text and Fig. 5 for details.

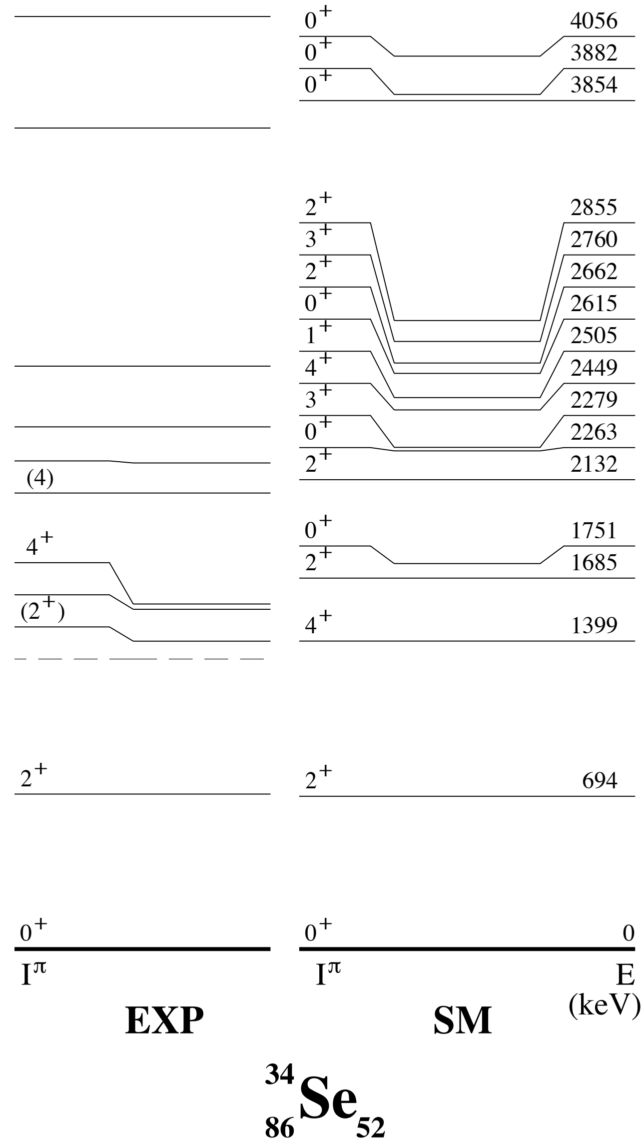


FIG. 9. Excited states in $^{86}$Se predicted in shell-model calculations (SM) in comparison with the results of this work (EXP). The vertical (energy) axis is plotted to scale. See text and Fig. 6 for details.

citation energy of the first $4^+$ level is explained within 200 keV. Its energy is slightly underestimated both in the present calculations and in those shown in Figure 19 of Ref. [21], pointing towards a problem with the interactions used so far away from the N=50 and Z=28 shell closure.

Calculations with the same model were proven to be rather robust and reliable for exotic, neutron-rich Ga isotopes [31]. The comparison of analogous predictions for $^{86}$As and $^{86}$Se with the experimental data discussed above, shows that the limit of their applicability might be reached when adding particles (5(6) protons and 3(2) neutrons, respectively) to the Z=28, N=50 doubly magic $^{78}$Ni core.

### B. Gamow-Teller decay of $^{86}$Ge and $^{86}$As

Very neutron-rich isotopes with N>50 and Z>28 are characterized by large $Q_\beta$ decay-energy window and low $S_n$ energy threshold in the daughter nuclei. In the single-particle limit, the allowed GT decays of these nuclei will proceed only between $fpg$ neutrons and the respective spin/orbit partner proton orbitals. The GT transformation of the valence neutrons, occupying the $d5/2$ and $s1/2$ orbitals are not possible in $\beta$ decay due to the limited $Q_\beta$

value. The $fpg$ neutron states that participate in the decay, are very deeply bound and, as a result, the GT decay transformation will populate mostly highly excited states. The lower-lying states will be fed in forbidden decays. This general picture emerges from the number of experimental results in this region of the chart of nuclei, [32–34].

The detailed analysis of the strength distribution can be related to the size of the N=50 shell gap. In the case of the N=50+2 isotope $^{82}$Zn, the analysis of its decay shows that the bulk of GT strength resides above the $S_n$ as determined by the shell gap of about 3.9 MeV [34]. Low-lying states, at about 2 MeV excitation energy, were identified with relatively low $logft$ value and were interpreted as $1^+$ states populated in the GT decay. This observation was interpreted as evidence of GT transitions to low-energy $1^+$ states proceeding through admixtures of the $d5/2^2((\pi f5/2)^2\ (\pi p3/2)^1,(\nu p1/2)^{-1})$ configuration with the main configuration $d5/2^2((\pi f5/2)^3,(\nu p1/2)^{-1})$. The latter configuration cannot be connected to the $^{82}$Zn ground state with the GT operator. This small portion of the GT-decay strength linked the $^{82}$Zn g.s. to the $^{82}$Ga neutron-bound states and was detected in traditional $\beta\gamma$ spectroscopy [34]. We expect a similar mechanism to be present in the decay of $^{86}$Ge.

Both $^{86}$Ge and $^{86}$As decay mostly to highly excited states and are characterized by large $P_n$ probabilities (45% and 35%, respectively). Nevertheless, there is a compelling evidence of GT decay to neutron-bound states in the daughter nuclei as shown in Figure 5. In order to continue the investigation of the role of the N=50 shell-gap into the decay of such exotic nuclei while departing further from the N=50 line, we have performed B(GT) calculations with NuShellX [16, 35]. An approach similar to the one that was developed to describe the results presented in [34] was used in the calculations. To model the $^{78}$Ni core decays, the calculations employed a $^{56}$Ni core and "blocking" of the valence neutrons in the $d5/2$ orbital to reduce the numerical complexity of the calculations. This approach is justified because at low excitation energies neutrons occupying these orbitals can be considered as spectators in the GT decay of $^{86}$Ge and $^{86}$As. Calculations were performed using a $^{56}$Ni core with the hybrid interaction and *nominal* single-particle energies (s.p.e.), as used in [34]: -8.39 MeV ($f5/2$), -8.54 MeV ($p3/2$), -7.21 MeV ($p1/2$), -5.86 MeV ($g9/2$) and -1.98 MeV ($d5/2$) for neutrons, and -14.94 MeV ($f5/2$), -13.44 MeV ($p3/2$), -12.04 MeV ($p1/2$) and -8.91 MeV ($g9/2$) for protons, as proposed by Grawe [36].

### 1. $^{86}$Ge.

The GT decay of the $0^+$ g.s. of $^{86}$Ge is going to populate $1^+$ states in the daughter nucleus $^{86}$As. The transformations energetically most favorable, thus with a large B(GT), will proceed via the $\nu p1/2\rightarrow\pi p3/2$ channel connecting the neutron and proton spin-orbit partners, which are closest to the Fermi energy. As in $^{82}$Zn, additional $1^+$ states could be also generated through $\nu p1/2\ (\pi f5/2)^n$ particle-hole configurations producing small B(GT) to them.

The experimental value for the apparent B(GT) feeding of the lowest ($1^+$) excited states in $^{86}$As with $logft\sim5$, corresponds to B(GT)$\sim$0.05 MeV$^{-1}$, see Figure 10. Our calculations with *nominal s.p.e.* produce a very large B(GT) to a $1^+$ level between 3 and 4 MeV (see Figure 10a) ) which is not observed experimentally and is different from the predictions for $^{82}$Zn decay. A closer inspection of the wavefunctions of the $1^+$ states involved in this decay reveals that here the configuration energetically most favorable is $(\nu p1/2)^{-1}\ (\pi f5/2)^4\ (\pi p3/2)^1$, which naturally results in a very large B(GT) due to the strong $\nu p1/2\rightarrow\pi p3/2$ transition.

Further investigations employed another set of interactions, which were constructed on the basis of *jj44bpn* [37] and *jj45pna* [30, 35]. These were developed for the $^{56}$Ni and $^{78}$Ni cores, respectively. Only the residual pn interactions between $sd$ neutrons and $fp$ protons are taken from *jj45pna* and the same method of calculation, with "blocking" of the neutrons in the $d5/2$ orbital, and s.p.e. were used as in Ref. [34]. The calculations which allowed scattering to the $s1/2$ orbital are possible, but they did not change the result significantly. This new hybrid set of interactions, should in principle be more reliable since the cross-shell matrix elements are not as "schematic" as in our previous work [34]. The results of this new set of calculations show a very large B(GT) between 2 and 3 MeV. This is due essentially to the same structure effects as in the previously used set of interactions, and again these theoretical predictions do not agree with the experimental data, see Figure 10. This result however illustrates the important role of the proton-neutron interactions in making reliable predictions of the decay strength distribution. Both sets of interactions predict that the decay will be dominated by the $\nu p_{1/2}\rightarrow\pi p_{3/2}$ transformation to a neutron-bound state in the daughter nucleus. In both cases, the shell model generates a strongly bound J=$1^+$ state with $(\pi f5/2)^4(\pi p3/2)\otimes(\nu d5/2)^4$ configuration. This situation is different for the decay of the N=52 $^{82}$Zn, where most likely the shell model predicts the lowest $1^+$ to be dominated by $(\pi f5/2)^3\otimes(\nu d5/2)^2$ configuration and small B(GT). In order to investigate a possible microscopic mechanism for this behavior, we have modified the T=0 elements of the residual interactions with the goal of achieving a qualitative agreement with experimental data. For this exercise, we used the interactions developed from *jj44bpn*. In order to push the $1^+$ state with large B(GT) above the neutron separation energy in $^{86}$Ge, we had to significantly weaken the diagonal T=0 matrix elements between $\nu d5/2$ and $\pi p3/2$ (by 1 MeV), which was generating the strongly bound $1^+$ state with large B(GT). Conversely, in order to generate low lying $1^+$ states with weak B(GT) the T=1 $\nu p1/2$ and $\pi f5/2$ had to be significantly strengthened, here by about 0.4 MeV. The results of the B(GT) calculations, with such modified interactions are shown in panel c) of Figure 10. One may notice, that now the $1^+$ states with large B(GT) are neutron unbound and the model is producing small B(GT) to the bound states in $^{86}$As, although the theoretical B(GT) is still much smaller than observed experimentally. We didn't continue further this empirical procedure. Interestingly this empirical modification, did not dramatically change the $^{82}$Zn result. A set of interactions with a better microscopic foundation needs to be developed to continue a more meaningful analysis. We merely emphasize the important role of the proton-neutron residual interactions in describing these very neutron-rich isotopes. The strong T=0 matrix elements might generate low-energy, doorway states which are neutron bound and could lead to dramatic increase of the decay lifetimes. In view of the experimental results, while we observe GT decays to states at low energies, with excitation energies lower than the shell gap, the B(GT) is very small and will not dramatically affect the nuclear lifetimes. A more complete empirical verification can be provided from $\beta$n spectroscopy which could identify directly the location of states with the large B(GT).

### *2.* $^{86}$*As.*

Excited states in $^{86}$Se with energies up to ~4.2 MeV were observed in the decay of $^{86}$As, and no obvious evidence of strong GT decays was detected. However, the states at high excitation energies could be populated by similar transitions as those observed at high excitation energies in the decay of $^{86}$Ge.

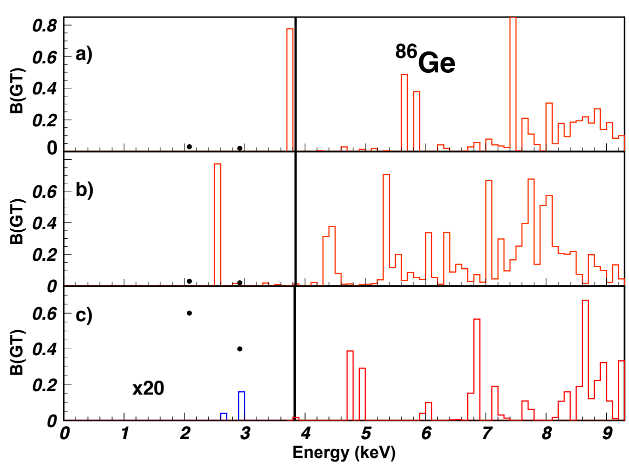


FIG. 10. (Color online) B(GT) strength distribution for $^{86}$Ge. The black dots represent the apparent B(GT) calculated from the present data and the histogram shows the results of the calculation. The part plotted in blue is multiplied by 20. All calculations use *nominal s.p.e.* and use a) interactions constructed from *jj44pn*; b) interaction constructed on the basis of the *jj45pn*; and c) as in a) but with modified T=0 parts interaction. The horizontal-axis represents $\beta$ energies from 0 to $Q_\beta$=9.2(3) MeV. The black vertical line highlights the $S_n$ value. See text for details.

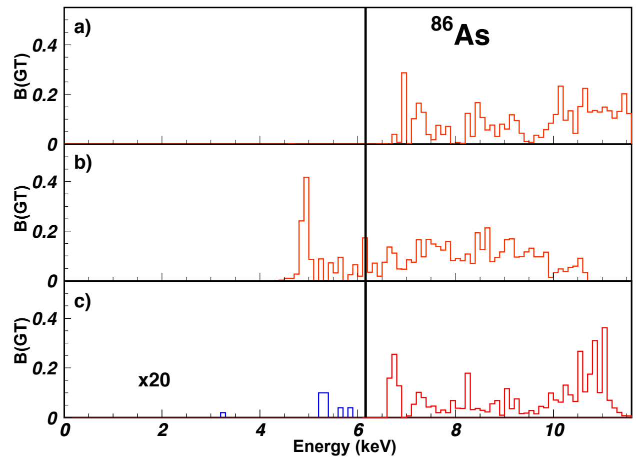


FIG. 11. (Color online) B(GT) strength distribution for $^{86}$As. The histogram shows the results of the calculation, the part plotted in blue is multiplied by 20. All calculations use nominal s.p.e. and use a) interactions constructed from *jj44pn*; b) interaction constructed on the basis of the *jj45pn*; and c) as in a) but with modified T=0 parts interaction. The horizontal-axis represents $\beta$ energies from 0 to $Q_\beta$=11.541(4) MeV. The black vertical line highlights the $S_n$ value. See text for details.

We performed the same calculations for $^{86}$As decay, as for $^{86}$Ge, assuming J=$2^-$ to be the ground state of $^{86}$As. The results are shown in Figure 11 for the same 3 scenarios. Similarly, for a) and b) the lowest energy strong B(GT) transitions can be traced back to $\nu p_{1/2} \rightarrow \pi p_{3/2}$ with the same microscopic mechanism. The empirical modification is necessary to reproduce the possible GT states below the neutron separation energy. Here, a new measurement, which would measure the absolute branching ratios below and above neutron separation energy is required, in order to make a more quantitative benchmarking of the model.

## V. SUMMARY AND OUTLOOK

The very neutron-rich isotopes $^{86}$Ge and its $\beta$-decay daughter $^{86}$As were produced in an experiment at the HRIBF and their $\beta$-decay properties were measured. First information on excited states populated in $^{86}$As by $^{86}$Ge $\beta$-decay was obtained, while the decay scheme of $^{86}$As to $^{86}$Se was largely extended. Comparison of the experimental data with shell-model calculations showed the limits of applicability for such calculations when departing from the double shell closure at N=50, Z=28. Calculations of GT strength highlighted the importance of the role of the proton-neutron residual interactions in describing these very neutron rich isotopes. Total $\gamma$ absorption and $\beta$-delayed neutron energy spectroscopy would be crucial to establish the true $\beta$ decay intensity pattern for $\beta$ decays of $^{86}$Ge and $^{86}$As. In particular, the direct $\beta$ feeding to the $^{86}$Se g.s. and $2^+$ excited states is needed to distinguish between the $(1^-)$ and $(2^-)$ assignments for the $^{86}$As ground state.

The very low production rate observed for $^{86}$Ge in the proton-induced fission of $^{238}$U together with the discrepancies in the fission yields for $^{86}$Ge reported in different data bases call for more accurate reactor yield measurements for this isotope [26, 38].

*Note.* While writing this paper we learned of a parallel work on the low-energy level scheme of $^{86}$Se [39].

We wish to acknowledge the Holifield Radioactive Ion Beam Facility (HRIBF) staff for their assistance with the experiments and providing excellent quality neutron-rich radioactive beams. This material is based upon work supported by the U.S. Department of Energy, Office of Science, Office of Nuclear Physics and this research used resources of the Holifield Radioactive Ion Beam Facility of Oak Ridge National Laboratory, which was a DOE Office of Science User Facility. This is supported in part under US DOE grants DE-AC05-00OR22725 (ORNL), DE-FG02-96ER40983 (UTK), DE-AC05-06OR23100 (ORAU), and DE-FG05-88ER40407 (Vanderbilt); in part by the National Nuclear Security Administration Grant No. DEFC03-03NA00143 and under the Stewardship Science Academic Alliance program through DOE Cooperative Agreement No. DE-FG52-08NA28552 (UTK).

[1] M. Bernas, S. Czajkowski, P. Armbruster, H. Geissel, Ph. Dessagne, C. Donzaud, H.ĐR. Faust, E. Hanelt, A. Heinz, M. Heese, C. Kozhuharov, Ch. Miehe, G. Munzenberg, M. Pfützner, C. Rohl, K.ĐH. Schmidt, W. Schwab, C. Stephan, K. Summerer, L. TassanĐGot, and B. Voss. *Phys. Lett.*, 331B:19, 1994.

[2] C. Mazzocchi, K.P. Rykaczewski, A. Korgul, R. Grzywacz, P. Bączyk, C. Bingham, N.T. Brewer, C.J. Gross, C. Jost, M. Karny, M. Madurga, A.J. Mendez II, K. Miernik, D. Miller, S. Padgett, S.V. Paulauskas, D.W. Stracener, M. Wolińska-Cichocka, and I.N. Borzov. *Phys. Rev. C*, 87:034315, 2013.

[3] C. Mazzocchi, A. Korgul, K.P. Rykaczewski, R. Grzywacz, P. Bączyk, C.R. Bingham, N.T. Brewer, C.J. Gross, C. Jost, M. Karny, M. Madurga, A.J. Mendez II, K. Miernik, D. Miller, S. Padgett, S.V. Paulauskas, D.W. Stracener, and M. Wolińska-Cichocka. *Acta Phys. Pol. B*, 46:713, 2015.

[4] M. Wang, G. Audi, A.H. Wapstra, F.G. Kondev, M. MacCormick, X. Xu, and B. Pfeiffer. *Chin. Phys. C*, 36:1603, 2012.

[5] J.R. Beene, D.W. Bardayan, A. Galindo Uribarri, C.J. Gross, K.L. Jones, J.F. Liang, W. Nazarewicz, D.W. Stracener, B.A. Tatum, and R.L. Varner. *J. Phys. G: Nucl. Part. Phys.*, 38:024002, 2011.

[6] R. Grzywacz. *Nucl. Instr. Methods in Phys. Res.*, B204:649, 2003.

[7] R. Grzywacz. *Nucl. Instr. Methods in Phys. Res.*, B261:1103, 2007.

[8] $http://www.xia.com/DGF\_Pixie-16.html$.

[9] J.P. Omtvedt, P. Hoff, M. Hellström, L Spanier, and B. Fogelberg. *Z. Phys.*, A338:241, 1991.

[10] A. Korgul et al., submitted to Phys. Rev. C.

[11] K. Miernik, K. P. Rykaczewski, C. J. Gross, R. Grzywacz, M. Madurga, D. Miller, J. C. Batchelder, I. N. Borzov, N. T. Brewer, C. Jost, A. Korgul, C. Mazzocchi, A. J. Mendez, Y. Liu, S. V. Paulauskas, D. W. Stracener, J. A. Winger, M. Wolińska-Cichocka, and E. F. Zganjar. *Phys. Rev. Lett.*, 111:132502, 2013.

[12] http://bricc.anu.edu.au/index.php.

[13] J. Kantele. Handbook of nuclear spectrometry, Academic Press Ltd., London, 1995.

[14] P.M. Endt. *At. Data Nucl. Data Tables*, 23:547, 1979.

[15] P.M. Endt. *At. Data Nucl. Data Tables*, 26:47, 1981.

[16] W. Rae, NUSHELLX shell-model code, http://www.garsington.eclipse.co.uk/.

[17] B. Singh, J.L. Rodriguez, S.S.M. Wong, and J.K. Tuli. *Nuclear Data Sheets*, 84:487, 1998.

[18] J. Agramunt et al. *Nuclear Data Sheets*, 120:74, 2014.

[19] J.V. Kratz, H. Franz, N. Kaffrell, and G. Herrmann. *Nucl. Phys. A*, 250:13, 1975.

[20] E.F. Jones, P.M. Gore, J.H. Hamilton, A.V. Ramayya, J.K. Hwang, A.P. deLima, S.J. Zhu, C.J. Beyer, Y.X. Luo, W.C. Ma, J.O. Rasmussen, I.Y. Lee, S.C. Wu, T.N. Ginter, M. Stoyer, J.D. Cole, A.V. Daniel, G.M. Ter-Akopian, and R. Donangelo. *Phys. Rev. C*, 73:017301, 2006.

[21] M. Czerwiński, T. Rząca-Urban, K. Sieja, H. Sliwińska, W. Urban, A.G. Smith, J.F. Smith, G.S. Simpson, I. Ahmad, J.P. Greene, and T. Materna. *Phys. Rev. C*, 88:044314, 2013.

[22] K. Tsukada, unpublished calculations based on data from Y. Zhao, Doctoral Thesis, Tokyo Metropolitan University, 1996.

[23] https://www-nds.iaea.org/exfor/endf.htm.

[24] J. Katakura, JENDL FP decay data file 2011 and fission yields data file 2011, $JAEA-Data/Code2011-025$, Japan Atomic Energy Agency, (2011).

[25] M. A. Kellet et al., The $JEFF-3.1/-3.1.1$ radioactive decay data and fission yields sub-libraries, $https://www.oecd-nea.org/dbdata/nds_jefreports/jefreport-20/nea6287-jeff-20.pdf$.

[26] G. Chiba, M. Tsuji, and T. Narabayashi. *Nuclear Data Sheets*, 118:401, 2014.

[27] T. Miyazono, M. Sagisaka, H. Ohta, K. Oyamatsu, and M. Tamaki. *Proceedings of the 1996 Symposium on Nuclear Data*, JAERI-Conf 97-005:83, 1997.

[28] http://www.nndc.bnl.gov/nudat2/fyields/.

[29] R. Machleidt, arXiv:0704.0807.

[30] M. Hjorth-Jensen, T. T. S. Kuo, and E. Osnes. *Physics Reports*, 261:125, 1995.

[31] R. Grzywacz, Gamow-Teller decays of nuclei beyond N>50, $22^{nd}$ ASRC International Workshop "Nuclear Fission and Exotic Nucle" Advanced Science Research Center (ASRC), Japan Atomic Energy Agency (JAEA), Tokai, Japan, December $3^{rd}$-$5^{th}$, 2014.

[32] J. A. Winger, John C. Hill, F. K. Wohn, R. L. Gill, X. Ji,

and B. H. Wildenthal. *Phys. Rev. C*, 38:285, 1988.
[33] S. Padgett, M. Madurga, R. Grzywacz, I. G. Darby, S. N. Liddick, S. V. Paulauskas, L. Cartegni, C. R. Bingham, C. J. Gross, K. Rykaczewski, D. Shapira, D. W. Stracener, A. J. Mendez II, J. A. Winger, S. V. Ilyushkin, A. Korgul, W. Królas, E. Zganjar, C. Mazzocchi, S. Liu, J. H. Hamilton, J. C. Batchelder, and M. M. Rajabali. *Phys. Rev. C*, 82:064314, 2010.
[34] M. F. Alshudifat et al., submitted to Physical Review C.
[35] B.A. Brown and W. Rae. *Nuclear Data Sheets*, 120, 2014.
[36] H. Grawe, Shell Model from a Practitioners Point of View, Lecture Notes I-II.
[37] B. Cheal, E. Mané, J. Billowes, M. L. Bissell, K. Blaum, B. A. Brown, F. C. Charlwood, K. T. Flanagan, D. H. Forest, C. Geppert, M. Honma, A. Jokinen, M. Kowalska, A. Krieger, J. Krämer, I. D. Moore, R. Neugart, G. Neyens, W. Nörtershäuser, M. Schug, H. H. Stroke, P. Vingerhoets, D. T. Yordanov, and M. Žáková. *Phys. Rev. Lett.*, 104:252502, 2010.
[38] A.A. Sonzogni, E.A. McCutchan, T.D. Johnson, and P. Dimitriou, to be published.
[39] T. Materna et al., *Phys. Rev. C*, 92:034305, 2015.